A Model for Flow in Meandering Streams

Article *in* Water Resources Research · September 1984

DOI: 10.1029/WR020i009p01301

CITATIONS
176

READS
275

2 authors, including:

Stephen Russell Mclean
University of California, Santa Barbara
45 PUBLICATIONS **3,896** CITATIONS

SEE PROFILE

WATER RESOURCES RESEARCH, VOL. 20, NO. 9, PAGES 1301–1315, SEPTEMBER 1984

A Model for Flow in Meandering Streams

J. DUNGAN SMITH

Geophysics Program, University of Washington, Seattle

S. R. MCLEAN

Department of Mechanical and Environmental Engineering, University of California, Santa Barbara

Erosion and deposition in streams and tidal channels depend on the divergence of the sediment-flux field, and this is governed by the distribution of boundary shear stress. As a consequence, erosion and deposition patterns in such systems are sensitive to spatial variations in boundary shear stress, which in turn, can be induced by the complex interplay between the flow and bed and bank topography. A method whereby variations in boundary shear stress can be calculated is presented herein for flows that are broad in relation to their depth and for which the bed slopes are small. The formal scheme employs a regular perturbation expansion around a zero-order state that includes vertically integrated, topographically induced convective accelerations. Use of a zero-order velocity field that includes these accelerative effects yields a model that is applicable to streams with typical bed slopes and channel curvatures, one that can be employed in the majority of situations of interest to geomorphologists, sedimentologists, and hydraulic engineers concerned with fluvial and estuarine systems. In order to verify the model, our calculations are shown to reproduce, with reasonable accuracy, the free-surface topography and boundary shear stress distribution measured by Hooke (1975) when applied to a channel of the geometry that he investigated. The latter part of the paper describes how the interplay of the various components of flow through a curved channel with bar-pool topography is affected by the parameters of the problem.

INTRODUCTION

Rivers and tidal channels in estuaries do not always follow straight paths; rather they often take on shapes characterized by sequences of smooth bends. Although segments of these bend sequences, or meanders, sometimes can be approximated using circular arcs, any general theory for flow through them must be able to accommodate lateral boundaries of arbitrary but slowly varying geometry. Furthermore, natural meandering streams have a characteristic bottom topography that must be accounted for in any theory to be used for the examination of flow structure and sediment-transport processes.

In this paper a model for the velocity, stress, and surface elevation fields in a meandering stream is presented. It is derived in an orthogonal, curvilinear coordinate system using a regular perturbation expansion around a zero-order state that employs the actual channel depth. In this manner the model can accommodate the specific geometry of most rivers. Topographic effects are included explicitly so the model can be applied to many sediment-transport problems and, in particular, so it can be used to evaluate the changes in channel geometry that occur as a river or tidal channel migrates. Models to be employed for the latter purpose must include convective accelerations induced by cross-stream and downstream variations in channel topography and by a changing radius of curvature because these can substantially alter local boundary shear stress, thus changing the pattern of erosion and deposition.

Two important attempts to model the effects of concern in this paper have been made previously, by Engelund and by DeVriend. In the first of these, the momentum fluxes associated with bar-pool topography and curvature were included in second order. The main differences between the results presented by Engelund and those described herein arise because (1) Engelund left out one of two equally important convective acceleration terms and (2) in most rivers with bar-pool topography the momentum flux terms are of primary, not secondary, importance [*Dietrich and Smith*, 1983].

The most recent work of DeVriend [e.g., *Kalkwijk and De-Vriend*, 1980; *DeVriend and Geldof*, 1983] is similar to ours in many respects. He emphasizes the effects of bar-pool topography and curvature; he uses a curvilinear rather than a modified cylindrical coordinate system, and he employs vertically integrated equations to develop the downstream velocity component field. The equations published by DeVriend, however, differ from ours in two respects. First, they do not include essential metrical coefficients, and second, they include terms that are not consistent with a systematic derivation of the governing equations for the meander problem. If the problem is solved numerically using the full momentum equations, then DeVriend's so-called secondary convection terms should be deleted, and if the equations to be solved are developed through a regular perturbation expansion, then these terms represent effects that belong in second order. In either case, the added terms are comparable in magnitude to second-order effects that have not been included, such as those resulting from neglected lateral stresses. Nevertheless, published velocity and boundary shear stress fields from DeVriend's model appear to be similar to the ones that our model would produce under the same conditions.

BASIC EQUATIONS

In order to simplify the equations for the meander problem as much as possible, we have chosen to use a right-handed, orthogonal, curvilinear coordinate system with the s axis aimed in the downstream direction and the near-vertical or z axis aimed upward. This means that the cross-stream or n axis must be positive outward on a bend with a negative radius of curvature. A single-valued coordinate system within the stream is guaranteed as long as the magnitude of the radius of curvature of the centerline $|R|$ is always greater than the distance from the centerline to the inside bank. Therefore the

Paper number 4W0460.
0043-1397/84/004W-0460$05.00

centerline of the channel should be selected to be as smooth as, or smoother than, the trace of the banks. For natural streams a suitably chosen $|R|$ is always greater than w_0, where w_0 is the mean width, so the condition that $|R|$ is greater than the distance from the channel centerline to the farthest bank will be fulfilled unless the banks are of an extremely unlikely geometry.

Using the definition sketch of Figure 1, the horizontal equations of motion for an appropriate curvilinear coordinate system can be derived using a single metrical coefficient based on a streamwise changing radius of curvature. This is done in the appendix. Writing the deviatoric stress components in terms of a spatially variable eddy viscosity yields equations (A8a) and (A8b), in which u_s, u_n, and u_z are the velocity components in the three curvilinear coordinate directions. The continuity equation transforms to

$$\frac{1}{(1-N)}\frac{\partial u_s}{\partial s} - \frac{u_n}{(1-N)R} + \frac{\partial u_n}{\partial n} + \frac{\partial u_z}{\partial z} = 0 \tag{1}$$

It should be noted that these equations also can be derived from the cylindrical coordinate version of the Navier-Stokes equations with spatially variable viscosity by substituting $(1-N)^{-1}\ \partial/\partial s = (1-n/R)^{-1}\ \partial/\partial s$ for $-(1/r)\ \partial/\partial\theta$, where r is the radial coordinate and θ is the tangential one. Various investigators have presented generalized versions of the horizontal momentum equations [e.g., *Engelund*, 1974]; however, none has shown that his generalized expressions include all of the terms necessary to characterize the flow through a bend of arbitrary channel geometry.

Owing to the gently sloping topography of normal river beds, it is sufficient to assume that vertical acceleration and vertical stress-induced forces per unit mass are small in comparison with the gravitational acceleration, so the third equation of motion is well approximated by the hydrostatic expression

$$-\frac{1}{\rho}\frac{\partial p}{\partial z} - g = 0 \tag{2}$$

Although this assumption breaks down in the immediate vicinity of steep banks adjacent to regions with significant cross-channel flow, these defects are local in nature and have a small effect on the overall flow pattern. In fact, they are not very significant even a short distance into the stream from the offending bank. To accommodate nonhydrostatic effects near these steep walls would complicate the theory substantially from a mathematical point of view without adding much new physical insight. Therefore the simpler model needs to be developed first and is the subject of this paper.

The hydrostatic equation (2) can be integrated from some level in the fluid to the free surface, $z = \sigma(s, n)$, where $p = p_\sigma$ to give $p = p_\sigma + \rho g(\sigma - z)$. Thus the horizontal pressure gradient $-\nabla p = -\rho g \nabla\sigma$ when $|\nabla p_\sigma| \ll |\rho g \nabla\sigma|$, as is the case in the problems of interest. In component form we have

$$-\frac{1}{(1-N)}\frac{\partial p}{\partial s} = \frac{-g}{(1-N)}\frac{\partial \sigma}{\partial s} \tag{3a}$$

and

$$-\frac{1}{\rho}\frac{\partial p}{\partial n} = -g\frac{\partial \sigma}{\partial n} \tag{3b}$$

both of which are independent of z.

Combining (A4), (A5), (A6), and (3), rearranging using (1), and integrating from the river bed η to the free surface σ leads to the following set of vertically integrated equations:

$$\rho\frac{1}{1-N}\frac{\partial}{\partial s}(\langle u_s^2\rangle h) + \rho\frac{\partial}{\partial n}(\langle u_s u_n\rangle h) - 2\frac{\rho\langle u_s u_n\rangle h}{(1-N)R}$$
$$= -\frac{\rho g h}{1-N}\frac{\partial \sigma}{\partial s} + \frac{1}{1-N}\frac{\partial}{\partial s}(\langle\tau_{ss}\rangle h)$$
$$+\frac{\partial}{\partial n}(\langle\tau_{ns}\rangle h) - \frac{2\langle\tau_{ns}\rangle h}{(1-N)R}$$
$$+\frac{1}{1-N}(\tau_{ss})_\eta\frac{\partial\eta}{\partial s} + (\tau_{ns})_\eta\frac{\partial\eta}{\partial n} - (\tau_{zs})_\eta \tag{4a}$$

$$\rho\frac{1}{1-N}\frac{\partial}{\partial s}(\langle u_s u_n\rangle h) + \rho\frac{\partial}{\partial n}(\langle u_n^2\rangle h) + \rho\frac{(\langle u_s^2\rangle - \langle u_n^2\rangle)h}{(1-N)R}$$
$$= -\rho g h\frac{\partial \sigma}{\partial n} + \frac{1}{1-N}\frac{\partial}{\partial s}(\langle\tau_{ns}\rangle h)$$

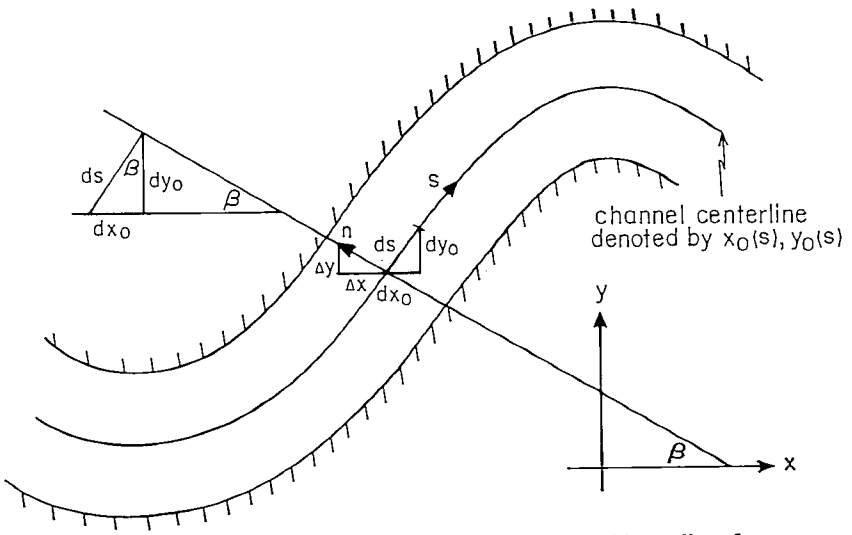

Fig. 1. Definition sketch for the curvilinear coordinate system in a bend of positive radius of curvature upstream and negative radius of curvature downstream. From the geometry we see that $\cos\beta = dy_0/ds$, $\sin\beta = dx_0/ds$, that $x = x_0 - \Delta x = x_0 - n\cos\beta = x_0 - n\,dy_0/ds$ and that $y = y_0 + \Delta y = y_0 + n\sin\beta = y_0 + n\,dx_0/ds$.

$$+\frac{\partial}{\partial n}(\langle\tau_{nn}\rangle h)+\frac{\langle\tau_{ss}-\tau_{nn}\rangle h}{(1-N)R}$$

$$+\frac{1}{1-N}(\tau_{ns})_\eta\frac{\partial\eta}{\partial s}+(\tau_{nn})_\eta\frac{\partial\eta}{\partial n}-(\tau_{zn})_\eta \qquad (4b)$$

where τ_{ij} are the components of the stress tensor in the curvilinear coordinate system and the subscript η denotes the value of the variable at the bed. Also, for steady flow, (1) integrates to

$$\frac{1}{1-N}\frac{\partial}{\partial s}(\langle u_s\rangle h)-\frac{\langle u_n\rangle h}{(1-N)R}+\frac{\partial}{\partial n}(\langle u_n\rangle h)=0 \qquad (5)$$

Here the angle brackets denote vertically averaged variables and h denotes the local flow depth.

SOLUTION FOR A MEANDERING RIVER

Application of the Vertically Integrated Equations

The next task is to ascertain the relative magnitudes of the various terms in the momentum and continuity equations. Unfortunately, multiple length scales characterize a meander bend. These are the mean flow depth h_0, the mean width w_0, the meander length m_0 measured from crossover to crossover along the centerline of the channel, and the minimum radius of curvature R_0. Three unique nondimensional numbers can be formed from these length scales, and we will use h_0/w_0, h_0/m_0, and h_0/R_0. In order to scale the momentum equations in a manner that will permit a single perturbation expansion it is necessary to constrain the values of these parameters relative to one another. Fortunately, the depth-to-width ratio is generally 0.1 or less, so $h_0/w_0 \ll 1$ can be assumed. The ratio of channel width to meander length is typically of order 0.1 also; thus $h_0/m_0 = O(h_0/w_0)^2$. The ratio of minimum radius of curvature to flow width ranges from 1.4 or so to ∞; thus $h_0/R_0 < h_0/w_0$. Here h_0/R_0 shall be assumed to be $O(h_0/w_0)$. In addition, the cross-stream velocity component and the cross-stream stress components are an order of magnitude smaller than the downstream ones, and the normal deviatoric stress components are small in comparison with $(\tau_{zs})_\eta$ and $(\tau_{zn})_\eta$.

As a consequence of these constraints, (4) reduces to

$$\frac{\rho}{1-N}\frac{\partial}{\partial s}\langle u_s^2\rangle h+\rho\frac{\partial}{\partial n}\langle u_s u_n\rangle h-2\rho\frac{\langle u_s u_n\rangle h}{(1-N)R}$$

$$=-\frac{\rho g h}{1-N}\frac{\partial\sigma}{\partial s}-(\tau_{zs})_\eta \qquad (6a)$$

$$\frac{\rho\langle u_s^2\rangle h}{(1-N)R}=-\rho g h\frac{\partial\sigma}{\partial n} \qquad (6b)$$

Dividing (6*b*) by h, then integrating with respect to n from the channel centerline, where $\sigma=\sigma_c$, differentiating with respect to s and multiplying by h yields

$$-\rho g h\frac{\partial\sigma}{\partial s}=-\rho g h\frac{\partial\sigma_c}{\partial s}-\rho\langle u_s^2\rangle h\frac{\partial}{\partial s}\ln(1-N)$$

$$-\rho h\int_0^{\ln(1-N)}\frac{\partial\langle u_s^2\rangle}{\partial s}\,d\ln(1-N) \qquad (7)$$

Substituting this equation into (6*a*) now produces the following expression for the boundary shear stress field:

$$(\tau_{zs})_\eta=-\frac{\rho g h}{1-N}\frac{\partial\sigma_c}{\partial s}$$

$$-\frac{\rho\langle u_s^2\rangle h}{(1-N)}\frac{\partial}{\partial s}\ln(1-N)-\rho\frac{\langle u_s^2\rangle}{1-N}\frac{\partial h}{\partial s}$$

$$-\frac{\rho h}{1-N}\left[\frac{\partial\langle u_s^2\rangle}{\partial s}-\int_0^N\frac{\partial\langle u_s^2\rangle}{\partial s}\frac{dN}{1-N}\right]$$

$$-\rho\frac{\partial}{\partial n}\langle u_s u_n\rangle h+2\rho\frac{\langle u_s u_n\rangle h}{(1-N)R} \qquad (8)$$

In principle, (8) can be used to calculate $(\tau_{zs})_\eta$ from flow measurements, but in practice it represents a delicate balance of large terms, some of which nearly cancel others. As a result, measurement and sampling errors make such an application difficult if not impossible. This point was clearly demonstrated by *Dietrich* [1982].

If $\partial\langle u_s^2\rangle/\partial s$ is slowly varying in N relative to $(1-N)^{-1}$, the integral in (8) is approximately $-(\partial\langle u_s\rangle/\partial s)\ln(1-N)$ so the term in brackets reduces to

$$\frac{\partial\langle u_s^2\rangle}{\partial s}[1+\ln(1-N)] \qquad (9)$$

However, $|N|\ll 1$, so $|\ln(1-N)|\ll 1$ and (9) is dominated by the first term, which means that the integral can be neglected without inducing serious error and that it can be included iteratively in a numerical solution if greater accuracy is required.

Dietrich's observations of flow in meandering streams suggest that $\langle u_s u_n\rangle \simeq \langle u_s\rangle\langle u_n\rangle$, except in the immediate neighborhood of pools. Therefore we shall use this approximation and employ (5) to find $\langle u_n\rangle$. Solving this first-order ordinary differential equation for $Q_n=\langle u_n\rangle h$ with $\langle u_n\rangle=0$ at $n=-b_1$ gives

$$\langle u_n\rangle h=-\frac{1}{1-N}\int_{-b_1}^{n}\left(\frac{\partial}{\partial s}\langle u_s\rangle h\right)dn \qquad (10)$$

Using

$$\frac{\partial}{\partial n}\langle u_n\rangle h=\frac{\langle u_n\rangle h}{(1-N)R}-\frac{1}{1-N}\frac{\partial}{\partial s}\langle u_s\rangle h \qquad (11)$$

and (10) in combination with the last two terms on the right side of (8) gives

$$-\rho\frac{\partial}{\partial n}\langle u_s u_n\rangle h+2\rho\frac{\langle u_s u_n\rangle h}{(1-N)R}$$

$$\simeq-\rho\langle u_s\rangle\frac{\partial\langle u_n\rangle h}{\partial n}-\rho\langle u_n\rangle h\frac{\partial\langle u_s\rangle}{\partial n}+2\rho\frac{\langle u_s\rangle\langle u_n\rangle h}{(1-N)R}$$

$$=\frac{\rho\langle u_s\rangle}{1-N}\frac{\partial}{\partial s}\langle u_s\rangle h$$

$$+\frac{\rho}{1-N}\frac{\partial\langle u_s\rangle}{\partial n}\int_{-b_1}^{n}\frac{\partial}{\partial s}\langle u_s\rangle h\,dn$$

$$-\frac{\rho\langle u_s\rangle}{(1-N)^2R}\int_{-b_1}^{n}\frac{\partial}{\partial s}\langle u_s\rangle h\,dn \qquad (12)$$

Now in order to close (8) and solve for $(\tau_{zs})_\eta$ we assume that $\langle u_s^2\rangle\simeq\langle u_s\rangle^2$ and $\rho\langle u_s^2\rangle=\alpha|\tau_{zs}|_\eta$, where $\alpha=O(10^2)$. This permits (12) to be transformed into

$$-\rho\frac{\partial}{\partial n}\langle u_s u_n\rangle h+2\rho\frac{\langle u_s u_n\rangle h}{(1-N)R}$$

$$\simeq\frac{\alpha|\tau_{zs}|_\eta}{1-N}\frac{\partial h}{\partial s}+\frac{1}{2}\left(\frac{h}{1-N}\right)\frac{\partial}{\partial s}(\alpha|\tau_{zs}|_\eta)$$

$$+\frac{1}{1-N}\frac{\partial(\alpha|\tau_{zs}|_\eta)^{1/2}}{\partial n}\int_{-b_1}^{n}\frac{\partial}{\partial s}(\alpha|\tau_{zs}|_\eta h^2)^{1/2}\,dn$$

$$-\frac{(\alpha|\tau_{zs}|_\eta)^{1/2}}{(1-N)^2R}\int_{-b_1}^{n}\frac{\partial}{\partial s}(\alpha|\tau_{zs}|_\eta h^2)^{1/2}\,dn \qquad (13)$$

and (8) to be written as

$$\left(\frac{1-N}{h}\right)(\tau_{zs})_\eta = -\rho g\frac{\partial\sigma_c}{\partial s}-\alpha|\tau_{zs}|_\eta\frac{\partial}{\partial s}\ln(1-N)-\frac{1}{2}\left(\frac{\partial\alpha|\tau_{zs}|_\eta}{\partial s}\right)$$

$$+\int_0^N\frac{\partial(\alpha|\tau_{zs}|_\eta)}{(1-N)\,\partial s}\,dN$$

$$+\frac{\partial(\alpha|\tau_{zs}|_\eta)^{1/2}}{\partial n}\frac{1}{h}\int_{-b_1}^{n}\frac{\partial}{\partial s}(\alpha|\tau_{zs}|_\eta h^2)^{1/2}\,dn$$

$$-\frac{(\alpha|\tau_{zs}|_\eta)^{1/2}}{(1-N)Rh}\int_{-b_1}^{n}\frac{\partial}{\partial s}(\alpha|\tau_{zs}|_\eta h^2)^{1/2}\,dn \qquad (14)$$

However, (14) has the form

$$\frac{\partial(\alpha|\tau_{zs}|_\eta)}{\partial s}+2\gamma_1(\alpha|\tau_{zs}|_\eta)=2\gamma_2 \qquad (15)$$

where

$$\gamma_1=\left(\sigma\frac{(1-N)}{\alpha h}+\frac{\partial}{\partial s}\ln(1-N)\right) \qquad (16a)$$

and

$$\gamma_2=-\rho g\frac{\partial\sigma_c}{\partial s}+\int_0^N\frac{\partial\alpha|\tau_{zs}|_\eta}{(1-N)\,\partial s}\,dN$$

$$+\frac{\partial(\alpha|\tau_{zs}|_\eta)^{1/2}}{\partial n}\frac{1}{h}\int_{-b_1}^{n}\frac{\partial}{\partial s}(\alpha|\tau_{zs}|_\eta h^2)^{1/2}\,dn$$

$$-\frac{(\alpha|\tau_{zs}|_\eta)^{1/2}}{(1-N)Rh}\int_{-b_1}^{n}\frac{\partial}{\partial s}(\alpha|\tau_{zs}|_\eta h^2)^{1/2}\,dn \qquad (16b)$$

In (16), σ is 1 when $(\tau_{zs})_\eta \geq 0$ and would be -1 if $(\tau_{zs})_\eta$ were negative. However $(\tau_{zs})_\eta$ will be negative only in separation zones, which encompass small parts of a bend, if any at all. Although (15) and (16) are valid for σ either positive or negative, the solution of (15) is not straightforward for cases where separation occurs; therefore this paper is restricted to situations for which separation does not occur. Assuming the terms in γ_2 with integrals in them are all small in relation to $|-\rho g\,\partial\sigma_c/\partial s|$ yields

$$|\tau_{zs}|_\eta=\exp\left(-\int_0^s 2\gamma_1\,ds\right)$$

$$\cdot\left[(\tau_{zs})_0+\frac{1}{\alpha}\int_0^s 2\gamma_2\exp\left(\int_0^s 2\gamma_1\,ds\right)ds\right] \qquad (17)$$

$$|\tau_{zs}|_\eta=(\tau_{zs})_0\left(\frac{1-N_0}{1-N}\right)\exp\left(-2\int_0^s\sigma\frac{1-N}{\alpha h}\,ds\right)$$

$$-\frac{2}{\alpha}\left(\frac{1-N_0}{1-N}\right)\exp\left(-2\int_0^s\sigma\frac{1-N}{\alpha h}\,ds\right)$$

$$\cdot\int_0^s\rho g\frac{\partial\sigma_c}{\partial s}\left(\frac{1-N}{1-N_0}\right)\exp\left(2\int_0^s\sigma\frac{1-N}{\alpha h}\,ds\right)ds \qquad (18)$$

in which $(\tau_{zs})_0$ represents the boundary shear stress at $s=0$ and N_0 represents the value of N there. Including the neglected terms of (16b) iteratively now permits a numerical solution of (14) for $|\tau_{zs}|_\eta$.

Defining a complete velocity field by

$$u_s=(u_*)_s f_1(\zeta,\zeta_0) \qquad (19)$$

where $(u_*)_s=[(\tau_{zs})_\eta/\rho]^{1/2}$ with $\zeta=(z-\eta)/(\sigma-\eta)=(z-\eta)/h$, and $\zeta_0=z_0/h$, where z_0 is the bottom roughness parameter, we find

$$\rho\langle(u_s)^2\rangle=(\tau_{zs})_\eta\int_{\zeta_0}^1 f_1{}^2\,d\zeta=\alpha(\tau_{zs})_\eta \qquad (20)$$

so

$$\alpha=\int_{\zeta_0}^1 f_1{}^2\,d\zeta \qquad (21)$$

To set the centerline slope, the streamwise component of discharge is held constant from cross section to cross section. That is,

$$\mathcal{Q}=Uw_0h_0=\int_{-b_1}^{b_2}h\int_{\zeta_0}^1(u_s\,d\zeta)\,dn \qquad (22)$$

or

$$\int_{-b_1}^{b_2}\hat{h}(\hat{u}_*)_s F_1\,d\hat{n}=1 \qquad (23)$$

where $\hat{u}_*=u_*/U_0$, $\hat{h}=h/h_0$, $\hat{b}_i=b_i/w_0$, and $\hat{n}=n/w_0$ and where

$$F_1=\int_{\zeta_0}^1 f_1\,d\zeta \qquad (24)$$

Once f_1 is specified, F_1 can be calculated from (24), and (23) can be solved iteratively by adjusting $\partial\sigma_c/\partial s$ until (23) is satisfied to the desired degree of accuracy. In practice, (14) is solved by assuming values of $(\tau_{zs})_\eta$ at $s=0$, then stepping downstream. The results are integrated across the stream to check (23), and the smaller terms are brought in iteratively. This calculation is done through several identical bends until the solution converges to the desired accuracy, the result being taken as the equilibrium condition. If the upstream conditions were known, only a single pass would be necessary, and if a section of river consists of several dissimilar bends, the solution is found by stepping through the bends consecutively.

Expansion and Separation of the Basic Equations

The analysis in the previous section comprises a simple model for the salient features of turbulent flow through a curved channel with an uneven bed. However, it also can be applied to the confined flow of materials such as mud, snow, and rock. The constitutive equation enters the problem solely through the specification of f_1, and thus only acts to set the numerical values of F_1 and α. Moreover, f_1, hence F_1 and α, is equally affected by the way in which the bed roughness is parameterized and the accuracy with which this is done for a particular problem of interest. Often the errors introduced through incomplete characterization of bed roughness are comparable to those caused by use of an oversimplified constitutive equation, and both can combine to negate any benefit from use of the local equations of motion. For avalanches and debris flows this may be the case, but when dealing with the

turbulent flow of water in rivers, estuaries, and canals, one can make some improvement by using the previous model as a zero-order state. This then is corrected for the various important effects that depend on vertical flow structure employing a regular perturbation expansion, governed by scaled versions of the full horizontal equations of motion.

Before proceeding with the perturbation expansion, it is desirable to rewrite the convective-acceleration terms in (A8*a*) as the $\mathbf{e}_s$ component of the divergence of the momentum-flux tensor, which is easily accomplished using the continuity equation (1) and yields

$$\begin{aligned}\frac{1}{1-N}u_s\frac{\partial u_s}{\partial s}+u_n\frac{\partial u_s}{\partial n}+u_z\frac{\partial u_s}{\partial z}-\frac{u_su_n}{(1-N)R}&\\ =\frac{1}{1-N}\frac{\partial}{\partial s}u_s^2+\frac{\partial}{\partial n}u_su_n+\frac{\partial}{\partial z}u_su_z-\frac{u_su_n}{(1-N)R}&\\ -u_s\left(\frac{1}{1-N}\frac{\partial u_s}{\partial s}+\frac{\partial u_n}{\partial n}+\frac{\partial u_z}{\partial z}\right)&\\ =\frac{1}{1-N}\frac{\partial}{\partial s}u_s^2+\frac{\partial}{\partial n}u_su_n+\frac{\partial}{\partial z}u_su_z-\frac{2u_su_n}{(1-N)R}&\end{aligned}\tag{25}$$

Now in order to scale (25) and (A8) we define the following nondimensional variables:

$$\hat{s}=\frac{s}{l_0}\qquad \hat{u}_s=\frac{u_s}{U}\qquad \hat{K}=\frac{K}{Uh_0}$$
$$\hat{n}=\frac{n}{w_0}\qquad \hat{u}_n=\frac{u_n}{U}\qquad \hat{R}=\frac{R}{R_0}\tag{26}$$

Here l_0 is the channel centerline between crossings. The scale velocity U is the river discharge divided by the mean meander width and the mean meander depth. The channel Froude number is

$$F_r=\frac{U}{(gh_0)^{1/2}}=\frac{\mathcal{Q}}{w_0h_0(gh_0)^{1/2}}\tag{27}$$

and it can be combined with l_0/m_0 to give $F_m=(m_0/l_0)^{1/2}F_r$. This latter parameter must be $O(1)$ because the flow is driven ultimately by the elevation difference of the free surface from crossing to crossing.

Finally, we let

$$\hat{u}_s=\hat{u}_s^{\,0}+\left(\frac{h_0}{w_0}\right)\hat{u}_s^{\,1}+\left(\frac{h_0}{w_0}\right)^2\hat{u}_s^{\,2}+\cdots\tag{28a}$$
$$\hat{u}_n=\hat{u}_n^{\,0}+\left(\frac{h_0}{w_0}\right)\hat{u}_n^{\,1}+\left(\frac{h_0}{w_0}\right)^2\hat{u}_n^{\,2}+\cdots\tag{28b}$$
$$\hat{u}_z=\hat{u}_z^{\,0}+\left(\frac{h_0}{w_0}\right)\hat{u}_z^{\,1}+\left(\frac{h_0}{w_0}\right)^2\hat{u}_z^{\,2}+\cdots\tag{28c}$$
$$\hat{\sigma}=\hat{\sigma}^0+\left(\frac{h_0}{w_0}\right)\hat{\sigma}^1+\left(\frac{h_0}{w_0}\right)^2\hat{\sigma}^2+\cdots\tag{28d}$$
$$\hat{K}=\hat{K}_0+\left(\frac{h_0}{w_0}\right)\hat{K}_1+\left(\frac{h_0}{w_0}\right)^2\hat{K}_2+\cdots\tag{28e}$$

where $\hat{u}_n^{\,0}=\hat{u}_z^{\,0}=\hat{u}_z^{\,1}=0$ and substitute the expressions from (3), (25), (26), (27), and (28) into (A8*a*) to get

$$\begin{aligned}\left(\frac{h_0}{m_0}\right)\frac{1}{1-N}\frac{\partial}{\partial\hat{s}}(\hat{u}_s^{\,0}\hat{u}_s^{\,0})+\left(\frac{h_0}{w_0}\right)^2\frac{\partial}{\partial\hat{n}}(\hat{u}_s^{\,0}\hat{u}_n^{\,1})&\\ +\left(\frac{h_0}{w_0}\right)^2\frac{\partial}{\partial\hat{z}}(\hat{u}_s^{\,0}\hat{u}_z^{\,2})-\left(\frac{h_0}{w_0}\right)\left(\frac{h_0}{R_0}\right)\frac{2\hat{u}_s^{\,0}\hat{u}_n^{\,1}}{(1-N)\hat{R}}&\\ =-\frac{F_m^{-2}}{1-N}\frac{\partial\hat{\sigma}^0}{\partial\hat{s}}-\left(\frac{h_0}{w_0}\right)\frac{F_m^{-2}}{1-N}\frac{\partial\hat{\sigma}^1}{\partial\hat{s}}-\left(\frac{h_0}{w_0}\right)^2\frac{F_m^{-2}}{1-N}\frac{\partial\hat{\sigma}^2}{\partial\hat{s}}&\\ -\left(\frac{h_0}{w_0}\right)\left(\frac{h_0}{R_0}\right)\frac{2\hat{K}_0}{(1-N)R}\frac{\partial\hat{u}_s^{\,0}}{\partial n}-\left(\frac{h_0}{R_0}\right)^2\frac{2\hat{K}_0\hat{u}_s^{\,0}}{(1-N)^2\hat{R}^2}&\\ +\left(\frac{h_0}{w_0}\right)^2\frac{\partial}{\partial\hat{n}}\hat{K}_0\frac{\partial\hat{u}_s^{\,0}}{\partial\hat{n}}+\left(\frac{h_0}{w_0}\right)\left(\frac{h_0}{R_0}\right)\frac{\partial}{\partial\hat{n}}\frac{\hat{K}_0\hat{u}_s^{\,0}}{(1-N)\hat{R}}&\\ +\frac{\partial}{\partial\hat{z}}\hat{K}_0\frac{\partial\hat{u}_s^{\,0}}{\partial\hat{z}}+\left(\frac{h_0}{w_0}\right)\frac{\partial}{\partial\hat{z}}\hat{K}_1\frac{\partial\hat{u}_s^{\,0}}{\partial\hat{z}}+\left(\frac{h_0}{w_0}\right)\frac{\partial}{\partial\hat{z}}\hat{K}_0\frac{\partial\hat{u}_s^{\,1}}{\partial\hat{z}}&\\ +\left(\frac{h_0}{w_0}\right)^2\frac{\partial}{\partial\hat{z}}\hat{K}_0\frac{\partial\hat{u}_s^{\,2}}{\partial\hat{z}}+\left(\frac{h_0}{w_0}\right)^2\frac{\partial}{\partial\hat{z}}\hat{K}_1\frac{\partial\hat{u}_s^{\,1}}{\partial\hat{z}}&\\ +\left(\frac{h_0}{w_0}\right)^2\frac{\partial}{\partial\hat{z}}\hat{K}_2\frac{\partial\hat{u}_s^{\,0}}{\partial\hat{z}}+O\left[\left(\frac{h_0}{w_0}\right)^3\right]&\end{aligned}\tag{29}$$

The superscripts on u_s, u_n, u_z, and σ represent orders, not powers. If such a variable is to be raised to a power, it will be enclosed in parentheses first. For all equations following (29), the same will be true of the analogous dimensional variables representing the various orders.

There are two zero-order terms and, when equated, they yield the governing equation for a steady, horizontally uniform current. In dimensional notation this relationship is

$$\frac{\partial}{\partial z}K_0\frac{\partial u_s^{\,0}}{\partial z}=\frac{g}{1-N}\frac{\partial\sigma^0}{\partial s}\tag{30}$$

Therefore for a flow with an unstressed upper surface the zero-order boundary shear stress must be related to the zero-order surface slope by $(1-N)(\tau_{zs}^{\,0})_\eta=-\rho hg\,\partial\sigma^0/\partial s$, and the stress profile must be

$$(\tau_{zs}^{\,0})=(\tau_{zs}^{\,0})_\eta(1-\zeta)\tag{31}$$

where $\zeta=(z-\eta)/h$.

In dimensional variables the first-order equation is

$$\frac{g}{1-N}\frac{\partial\sigma^1}{\partial s}=\frac{\partial}{\partial z}\left(K_0\frac{\partial u_s^{\,1}}{\partial s}+K_1\frac{\partial u_s^{\,0}}{\partial s}\right)\tag{32}$$

and the second-order expression for a conservation of momentum becomes

$$\begin{aligned}\frac{1}{1-N}\frac{\partial}{\partial s}(u_s^{\,0}u_s^{\,0})+\frac{\partial}{\partial n}(u_s^{\,0}u_n^{\,1})+\frac{\partial}{\partial z}(u_s^{\,0}u_z^{\,2})-\frac{2(u_s^{\,0}u_n^{\,1})}{(1-N)R}&\\ =-\frac{g}{1-N}\frac{\partial\sigma^2}{\partial s}-\frac{2K_0u_s^{\,0}}{(1-N)^2R^2}-\frac{2K_0}{(1-N)R}\frac{\partial u_s^{\,0}}{\partial n}&\\ +\frac{\partial}{\partial n}\frac{K_0u_s^{\,0}}{(1-N)R}+\frac{\partial}{\partial n}K_0\frac{\partial u_s^{\,0}}{\partial n}+\frac{\partial}{\partial z}K_1\frac{\partial u_s^{\,1}}{\partial z}&\\ +\frac{\partial}{\partial z}K_0\frac{\partial u_s^{\,2}}{\partial z}+\frac{\partial}{\partial z}K_2\frac{\partial u_s^{\,0}}{\partial z}&\end{aligned}\tag{33}$$

As will be shown below, if all of the discharge is accounted for in the zero order, K_1, $u_s^{\,1}$, and $\partial\sigma^1/\partial s$ must be zero.

The scaled and expanded version of (A8*b*) is

$$\left(\frac{h_0}{R_0}\right)\frac{(\hat{u}_s{}^0)^2}{(1-N)\hat{R}}+\left(\frac{h_0}{R_0}\right)\left(\frac{h_0}{w_0}\right)\frac{2\hat{u}_s{}^0\hat{u}_s{}^1}{(1-N)\hat{R}}$$
$$=-\left(\frac{m_0}{w_0}\right)F_m{}^{-2}\frac{\partial\hat{\sigma}^0}{\partial\hat{n}}-\left(\frac{m_0}{w_0}\right)\left(\frac{h_0}{w_0}\right)F_m{}^{-2}\frac{\partial\hat{\sigma}^1}{\partial\hat{n}}$$
$$-\left(\frac{m_0}{w_0}\right)\left(\frac{h_0}{w_0}\right)^2F_m{}^{-2}\frac{\partial\hat{\sigma}^2}{\partial\hat{n}}+\left(\frac{h_0}{w_0}\right)\frac{\partial}{\partial\hat{z}}\hat{K}_0\frac{\partial\hat{u}_n{}^1}{\partial\hat{z}}$$
$$+\left(\frac{h_0}{w_0}\right)^2\frac{\partial}{\partial\hat{z}}\hat{K}_0\frac{\partial\hat{u}_n{}^2}{\partial\hat{z}}+\left(\frac{h_0}{w_0}\right)^2\frac{\partial}{\partial\hat{z}}\hat{K}_1\frac{\partial\hat{u}_n{}^1}{\partial\hat{z}}$$
$$+O\left(\left[\frac{h_0}{w_0}\right]^3\right) \tag{34}$$

In (34) the terms containing $\partial\sigma^0/\partial n$ and $\partial\sigma^1/\partial n$ are unopposed and must then be set equal to zero. As a consequence there is no first-order cross-stream flow component. The lowest order cross-stream equation of motion is

$$\frac{(u_s{}^0)^2}{(1-N)R}=-g\frac{\partial\sigma^2}{\partial n}+\frac{\partial}{\partial z}K_0\frac{\partial u_n{}^1}{\partial z} \tag{35}$$

This expression is analogous to the first-order equation derived in cylindrical coordinates for a circular annulus then applied to meandering streams by *Rozovskii* [1957] and *Yen* [1972]. However, neither of these authors relates the surface elevation in the downstream equation of motion to that in the cross-stream momentum equation, so they count orders with respect to velocity, not to surface elevation as we must do here. Equation (35) is a first-order expression in terms of velocity.

Calculations carried to second order using the basic force balance developed above clearly indicate that accelerative effects must be included at the lowest order if problems in which the bed has significant topographic structure or in which the channel has significant curvature are to be addressed. This conclusion has been confirmed by computations employing the simple model of the preceding section. Also it is consistent with the experimental findings of *Yen and Yen* [1971] and *Hooke* [1975] and with our field measurements [see *Dietrich*, 1982], all of which are for beds of equilibrium or near-equilibrium geometry. Therefore to produce a model of reasonable generality, it is necessary to include vertically integrated convective accelerations in the zero order.

In order to accomplish this task we rewrite (14) in terms of zero-order variables, use the fact that there is no first-order flow (with respect to the surface-elevation expansion), and calculate the second-order cross-stream velocity field from a modified version of (35). Use of a different zero order does not introduce a nonzero first-order velocity field, but it does have a substantial and complicated effect on the second-order flow, so in the present analysis the expansion will be terminated before this difficulty arises.

Owing to the inclusion of the effects of a cross-stream free-surface slope in (14) via (6*b*), it must be assumed that there is a zero-order cross-stream equation of motion of the form

$$\frac{\langle(u_s{}^0)^2\rangle}{(1-N)R}=-g\frac{\partial\sigma_*{}^0}{\partial n} \tag{36}$$

and that this must be removed from the second-order expression with respect to this surface-elevation expansion, yielding

$$\frac{(u_s{}^0)^2-\langle(u_s{}^0)^2\rangle}{(1-N)R}=-g\frac{\partial\sigma_*{}^2}{\partial n}+\frac{\partial}{\partial z}K_0\frac{\partial u_n{}^1}{\partial z}$$

where

$$\partial\sigma_*{}^2/\partial n=\partial\sigma^2/\partial n-\partial\sigma_*{}^0/\partial n \tag{37}$$

When (36) and (37) are added together, they give (35).

This alteration of the perturbation expansion does not seriously violate the basic premise because it produces no zero-order cross-stream flow and because $[(u_s{}^0)^2-\langle(u_s{}^0)^2\rangle]$ is small in relation to $\langle(u_s{}^0)^2\rangle$ throughout most of the flow depth. In fact in (35) the left-hand side and the first term on the right-hand side are almost in balance, so shifting the two terms to zero order is clearly justified. If the expansion were to be carried to second order in the downstream equation of motion as well, then (33) would have to be altered in an analogous manner in order to permit the vertically averaged momentum-flux-divergence terms to be moved to zero order.

The Zero- and First-Order Velocity Fields

No matter which zero-order solution is chosen, the only term that could depend on ζ is $\partial\tau_{zs}{}^0/\partial\zeta$, so (31) still pertains and $\tau_{zs}{}^0=\rho(u_*{}^0)^2(1-\zeta)=\rho K_0\partial u_s{}^0/\partial z$. Taking $K_0=u_*{}^0h\kappa$, where $\kappa=\kappa(\zeta)$, gives $\partial u_s{}^0/\partial\zeta=u_*(1-\zeta)/\kappa$, which integrates to

$$u_s{}^0=u_*{}^0\int_{\zeta_0}^{\zeta}\frac{(1-\zeta)}{\kappa}\,d\zeta=u_*{}^0f_1(\zeta,\zeta_0) \tag{38}$$

In addition, (32) yields

$$u_s{}^1=(u_*{}^1)_sf_1(\zeta,\zeta_0) \tag{39}$$

The discharges per unit width associated with these velocity fields are $Q_s{}^0=(u_*{}^0)_shF_1$ and $Q_s{}^1=(u_*{}^1)_shF_1$, where

$$F_1=\int_{\zeta_0}^{1}f_1\,d\zeta=\int_{\zeta_0}^{1}\int_{\zeta_0}^{\zeta}\frac{1-\zeta'}{\kappa}\,d\zeta' \tag{40}$$

All of the volume discharge is accounted for in zero order, and σ^1 is independent of n as shown above; therefore $Q_s{}^1=0$, $(u_*{}^1)_s=0$ and $\partial\sigma^1/\partial s=0$.

The Second-Order Velocity Field

In order to find the cross-stream velocity component $u_n{}^1$ we substitute for $u_s{}^0$ in (35) and integrate twice with respect to z, using the boundary conditions that $\partial u_n{}^1/\partial z=0$ at $\zeta=1$ and $u_n{}^1=0$ at $\zeta=\zeta_0$. We then apply the constraint provided by $Q_n{}^1$ to set $\partial\sigma^2/\partial n$. This yields the standard vertical velocity profile for the secondary circulation [cf. *Rozovskii*, 1957; *Yen*, 1965, 1972] but gives a more complicated horizontal structure to the cross-stream component of the flow. After the first substitution, (35) becomes

$$\frac{\partial}{\partial z}K_0\frac{\partial u_n{}^1}{\partial z}=g\frac{\partial\sigma^2}{\partial n}+\frac{(u_*{}^0)_s{}^2}{(1-N)R}f_1{}^2 \tag{41}$$

When integrated twice with the above-mentioned limits, (41) yields

$$u_n{}^1=\frac{1}{(u_*{}^0)_s}\left(-\frac{(u_*{}^0)_s{}^2h}{(1-N)R}f_2-gh\frac{\partial\sigma^2}{\partial n}f_1\right) \tag{42}$$

where

$$f_2(\zeta)=\int_{\zeta_0}^{\zeta}\frac{1}{\kappa}\int_{\zeta'}^{1}f_1{}^2\,d\zeta''\,d\zeta' \tag{43}$$

Now applying the condition from (10) that

$$Q_n^1 = \frac{-1}{1-N}\int_{-b_1}^{n} \frac{\partial Q_s^0}{\partial s}\,dn = -\frac{1}{1-N}\int_{-b_1}^{n}\left[\frac{\partial}{\partial s}(u_*^0)_s h F_1\right] dn \tag{44}$$

gives

$$-g\frac{\partial \sigma^2}{\partial n} = \frac{(u_*^0)_s^2}{(1-N)R}\frac{F_2}{F_1} - \frac{(u_*^0)_s}{(1-N)h^2F_1}\int_{-b_1}^{n}\left[\frac{\partial}{\partial s}(u_*^0)_s h F_1\right] dn \tag{45}$$

where

$$F_2 = \int_{\zeta_0}^{1} f_2\,d\zeta = \int_{\zeta_0}^{1}\int_{\zeta_0}^{\zeta'}\frac{1}{\kappa}\int_{\zeta}^{1} f_1^2\,d\zeta'''\,d\zeta''\,d\zeta' \tag{46}$$

so

$$u_n^1 = \frac{(u_*^0)_s h}{(1-N)R}\left(\frac{F_2}{F_1}f_1 - f_2\right) - \left\{\frac{1}{(1-N)hF_1}\int_{-b_1}^{n}\left[\frac{\partial}{\partial s}(u_*^0)_s h F_1\right] dn\right\} f_1 \tag{47}$$

and

$$\tau_{zn}^1 = \frac{\rho(u_*^0)_s h}{(1-N)R}\left[\frac{F_2}{F_1}(1-\zeta) - \int_{\zeta}^{1} f_1^2\,d\zeta\right] - \frac{\rho(u_*^0)_s(1-\zeta)}{(1-N)hF_1}\int_{-b_1}^{n}\left[\frac{\partial}{\partial s}(u_*^0)_s h F_1\right] dn \tag{48}$$

In principle these calculations can be carried to higher order, but the predominant features of the modeled flow are included in the second-order calculation. Eventually, effects that have not been and perhaps cannot be treated with the general approach taken in this paper become of comparable magnitude to the higher-order corrections. Examples of such effects are nonhydrostatic responses to abrupt changes in bed topography, complications due to lateral boundary layers near steep banks, horizontal accelerative effects due to abrupt changes in bank and bed topography, and perhaps most important, spatial changes in the turbulent structure of the flow interior due to advective processes. Of particular importance in regard to turbulence production are boils associated with three-dimensional bed forms because they cause substantially enhanced momentum and mass transfer in the interior of the flow above and downstream of the vorticity-generating dune fields.

APPLICATION OF THE MODEL

Choice of Appropriate Geometric Constraints

Langbein and Leopold [1966] argue that natural rivers follow channels that closely approximate sine-generated curves. For this reason, *Hooke* [1975] employed a sine-generated curve in his flume experiments, and we shall use this geometry in the test cases presented in this paper. As pointed out in the introduction, our model can accommodate a wide variety of centerline paths of streams, but it is necessary to put some constraints on the centerline that is used in order to examine the relative importance of other, more essential effects. Also, for the latter reason, only channels with parallel banks will be modeled.

If ϕ is the local derivation of the channel centerline path from a line parallel to the down-valley direction, then a sine-generated curve is represented by the equation

$$\phi = \omega \cos \pi s/m_0 \tag{49}$$

where ω is the value of ϕ as it crosses the down-valley axis and m_0 is the half wavelength measured along the channel centerline. The radius of curvature for a sine-generated curve is expressed by

$$R = \left(\frac{d\phi}{ds}\right)^{-1} = \left(\frac{\pi\omega}{m_0}\sin\frac{\pi s}{m_0}\right)^{-1} \tag{50}$$

This gives a plan geometry that is characterized by two parameters: w_0/m_0 and ω. Most of the calculations presented in this paper are in the format of vector ("stick") diagrams plotted at various cross sections in a half-wavelength segment of a sine-generated curve. These segments are compared at the same wavelength and display the correct width-to-wavelength ratio.

The model presented in this paper was developed for the purpose of calculating boundary shear stress in sediment-transporting rivers and estuaries. In erodible-boundary systems of this type the bottom takes on a characteristic cross-stream geometry, one with relatively flat beds in the neighborhoods of crossings and with steeply sloping beds in the sharpest parts of the bends. In the latter locations, pools due to divergent sediment fluxes form on the outsides, and bars due to convergent sediment fluxes form on the insides. A similar bed morphology was employed in a valuable set of flume experiments carried out by *Hooke* [1975], and the flow data presented by Hooke provide an ideal case against which to test our model. Figure 2 shows the measured bottom topography and a map of boundary shear stress for Hooke's stabilized bed run, presented in combination with our predicted boundary shear stress. From Figure 2*a* the channel cross sections can be seen to be approximately rectangular in the crossings and nearly triangular in the center of the bend, where the characteristic bar-pool morphology is best developed. For this experiment, $\omega = 55$, $h_0/w_0 = 0.091$, $w_0/m_0 = 0.014$, $h_0 = 0.092$ m, and $U = 0.38$ m/s; the average boundary shear stress was 0.80 N/m^2.

Comparison of Calculated and Measured Variables

The first detailed comparison between model and experiment is presented in Figure 3. Here the channel-centerline-surface elevation is used to evaluate the ability of the model to account for the salient, topographically induced, nonlinear effects that restrict the flow in the neighborhood of the bend. These effects cause a steep surface slope near each bend while producing relatively flat surface topography in the vicinity of the crossings. For a given surface slope, increasing the velocity over the bar and reducing it over the pool, relative to the situation that would arise if only the depth-slope product term were important, reduce the discharge. Therefore in order to maintain a constant discharge at every cross section the surface slope must steepen near the section where the bar-pool topography is best developed (i.e., near the sharpest part of the bend for the Hooke experiment). The resulting backwater curve then reduces the slope in the neighborhood of the crossings.

The convective accelerations that cause the flow to increase

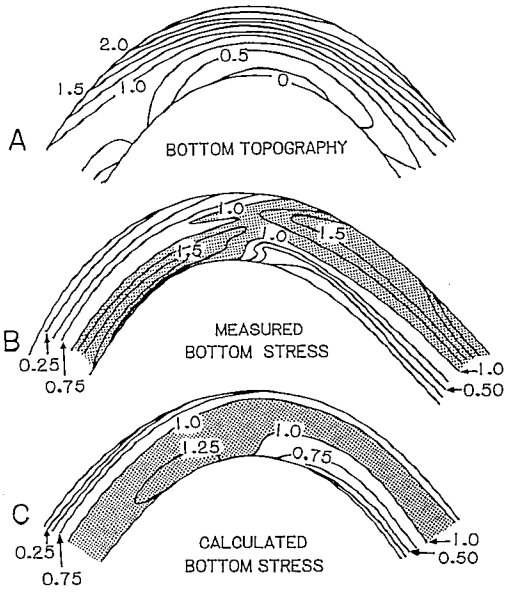

Fig. 2. Comparison of (*b*) measured and (*c*) calculated boundary shear stress fields for flow through a channel with the bottom topography established in Hooke's flume, run 35S (*a*). Bed elevation contours are nondimensionalized by the mean depth, which was 0.092 m, and the boundary shear stress is normalized by the average measured value (0.80 N/m^2). The parameters for this calculation are $\omega = 55°$, $h_0/w_0 = 0.091$, $h_0/m_0 = 0.014$, $z_0/h_0 = 1.0 \times 10^{-3}$, and $\kappa = k\zeta(1 - \zeta)^{1/2}$.

over the point bar and decrease over the pool are, in fact, largest upstream of the point bar crest and pool trough. Thus the zone of steepest centerline slope is shifted upstream from the minimum radius of curvature. This effect is evident in both the theoretical curve and the experimental data plotted in Figure 3. Moreover, these accelerations are greater on the inside of the bend than on the outside; thus the region of steepest slope is farther upstream on the inside of the stream than on the outside. In contrast, in a flat-bedded stream the centerline surface slope is independent of along-channel position, as shown experimentally by *Yen and Yen* [1971], and as has been verified by our model.

Superimposed on the topographically induced nonlinear response is an already well-described and well-understood cross-stream elevation change produced by the cross-stream pressure-gradient force, vertically averaged centrifugal force balance of (36). As the centerline curvature increases, so does the cross-stream slope. If the change in curvature is large, the resulting increase in surface elevation along the outside bank can balance or even exceed the downstream slope there. In rivers with typical bed topography this often occurs near the crossings because $\partial R/\partial s$ is maximum there, while the downstream centerline slope at this location is usually quite small for the reason given in the previous two paragraphs. In contrast, these effects combine to produce a relatively steep slope on the down-valley side of the crossing. The downstream slope also is steeper on the inside of the bend than on the outside because it is a shorter distance from crossing to crossing there; however, this effect is maximum at the radius-of-curvature minimum, not at the crossing. When all three of these components are added together, the resultant free-surface topography is as shown in Figure 4*d*. Of particular note here are the flat regions on the up-valley sides of the stream near the crossings and steep slopes on the down-valley sides, especially upstream of the point bar.

Many of the characteristics of flow through a moderate bend with typical natural topography are represented by the stick diagrams in Figure 4. Of special importance in sediment-transport problems is the pattern of boundary shear stress, which is shown in two separate ways. The magnitude of this vector field is presented in Figure 4*a* so that the features associated with the maximum-value zone, as it shifts from near the inside bank in the upstream crossing to near the outside bank below the radius-of-curvature minimum, can be seen clearly. In particular, Figure 4*a* permits the broad, weakly double-peaked, high shear stress region in the neighborhood of the curvature maximum to be discerned. This feature is much less obvious in the full vector diagram of Figure 4*b* due to the orientation of the vectors. In contrast, the vector directions are necessary to show the weak outward component of stress in the neighborhood of the crossing, the changeover, then the increasing inward stress component as the bend sharpens, and finally the maintenance of this inward component all the way to the next crossing.

Figure 4*b* also clearly demonstrates the concentration of the so-called secondary circulation over the pool, as well as the weak outward component of boundary shear stress over the top of the point bar. The latter is the result of a downstream, convective-acceleration-induced rise in free-surface elevation over the point bar. This varies laterally and, being greatest at the inner bank, it counteracts the cross-stream surface slope that would result from the centrifugal force alone, thereby causing a weak outward cross-stream flow near the inner bank. This is opposite to what would be predicted if the downstream and cross-stream pressure fields were not coupled or if topographically induced convective accelerations were not included. The outward flow at this location and its geomorphological ramifications have been examined in detail by *Dietrich and Smith* [1983] using field and laboratory data.

Contour diagrams of Hooke's measured and our calculated boundary shear stress magnitudes are presented in Figures 2*b* and 2*c*, respectively. The same general pattern is displayed by both. For example, comparing the calculated and measured 1.0 contours indicates a region of high boundary shear stress centered about one-quarter of the way out from the inside bank between the upstream crossing and the center of the bend, and a similar band centered about one-quarter of the way in from the outer bank between the center of the bend and the downstream crossing. These zones of high boundary shear stress are connected by a broad region of nearly uniform boundary shear stress over the top of the point bar. Bands of low boundary shear stress are found along the outer bank upstream of the pool and along the inner bank downstream of the point bar crest. In essence, these figures both show a band of high bottom stress extending from the downstream end of

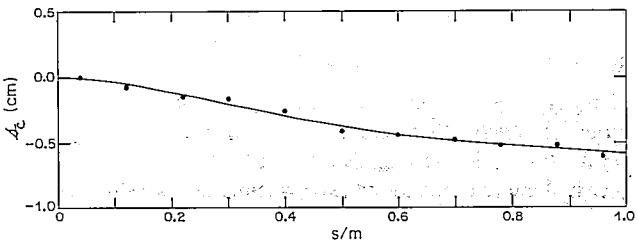

Fig. 3. Comparison of measured (dots) and calculated (line) centerline free-surface elevation for Hooke's fixed bed run. For a flat bedded channel with the same plane geometry the free-surface elevation would vary linearly between the two end points (crossings).

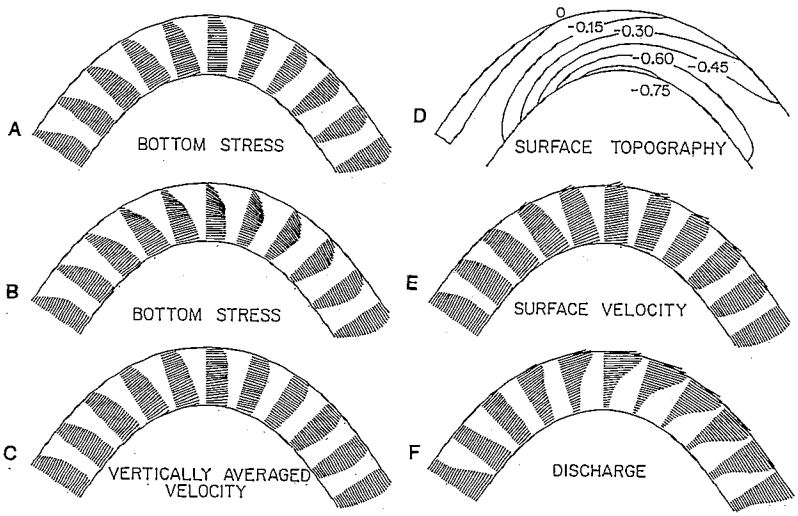

Fig. 4. Fields of important flow variables as calculated for the conditions of Hooke's fixed bed run. Except for the contour diagram of free surface elevation (Figure 4*d*), all fields are displayed in stick form. The length of each stick represents the magnitude of the variable at the origin, and the orientation of the stick yields the direction of the vector quantity. The reference point is on the straight section to the left. Owing to its importance, boundary shear stress is displayed both as a scalar field (*a*) using magnitude only and (*b*) in vector form. The bar scale at the bottom of the figure gives the unit magnitude for the normalized variables. The scale factors are (*a* and *b*) ρU^2, (*c* and *e*) U, and (*f*) Uh_0. Surface elevation (*d*) is contoured in centimeters relative to an arbitrary datum.

the pool to the top of the next point bar and a zone of low bottom stress extending from just below the crest of the point bar into the next pool. Inertial effects had to be taken into account in order to model these important zones.

There are two main differences between the measured and calculated bottom stress fields. First, boundary shear stress maxima are underestimated by the model because the closure condition $(\tau_{zs})_\eta = \alpha\langle u_s\rangle^2$ does not account for enhancement of the stress field in regions of accelerating flow and reduction of it in regions of decelerating flow. Including the second-order downstream equation of motion in the expansion would rectify this difficulty. Second, the calculated zone of low boundary shear stress extends too far downstream along the outer bank. This difficulty is due to the complete exclusion of lateral mixing effects in zero order, and it can be at least partially corrected by including the second-order, downstream equation of motion in the perturbation expansion. Nevertheless, treatment of lateral mixing in the basic formulation of the problem is oversimplified, so the inclusion of lateral boundary layers in regions with steep banks may be necessary if high accuracy is desired at these locations.

The magnitudes of the two stress fields may be made to agree precisely by adjusting the effective roughness parameter within the probable error of assessing the actual hydraulic roughness of the bed. Calculation of the roughness parameter (z_0) must be done such that form drag on all but the features displayed in the topographic map of Figure 2*a* is included in a single, spatially averaged roughness parameter. Of course, if data on the local variability of the roughness length were available, these data could be included in the model, but in the case of interest they were not. We estimated a mean value of $z_0 = 0.9 \times 10^{-4}$ m from Hooke's description of his experimental procedure.

Examination of the surface-velocity field in combination with the bottom-stress distribution of Figure 4*b* provides the angular difference between the flow directions in the vicinity of the upper and lower boundaries of the stream. This measure of so-called "helical flow intensity" also indicates that secondary circulation is best developed over the pool. Moreover, a helical component to the flow can be seen to be nonexistent near the crossings and small over the top of the point bar. A general outward direction to the flow between the upstream crossing and the center of the bend and then a general inward component also can be seen from joint examination of these two figures. However, this topographically induced tendency for the high-velocity core of the flow to move from pool to pool is better indicated by the vertically averaged velocity field presented in Figure 4*c*. It is the cause of the pronounced variation in discharge per unit width displayed in the adjacent panel, and it is a direct consequence of (10). This crossing of the high-velocity core from the inner to outer bank is a frequently observed feature of flow in natural bends.

In spite of the above-noted differences, the agreement between calculated and measured parameters certainly is acceptable for many sedimentological and geomorphological purposes, justifying use of the model as an interpretive and predictive tool. Of course, further comparisons with comprehensive measurements made in flow through bends of typical fluvial geometry are required, and one such test already is planned for the data set described by *Dietrich* [1982]. Although inclusion of effects arising from the second-order streamwise equation of motion appears worthwhile, the predominant features of the modeled flows are not likely to change too much, and it seems desirable to use the version at hand to examine the variation of salient flow characteristics with important stream parameters in order to gain some insight regarding the mechanics of natural streams.

Variation of Model Results With Important Parameters

It has been argued previously in this paper that large-scale bed morphology is of fundamental (zero-order) importance; therefore it is reasonable to examine the change in flow response as Hooke's topography is reduced in amplitude while the banks are kept in their original position. Reduction of the amplitude of the bottom topography to zero leaves a flat-bedded channel of the same plane geometry but with vertical

walls. This topography modification has been carried out in several steps so that the change in flow characterisics can be traced easily. Bottom stress, surface velocity, and discharge fields for reduction ratios of $H_0/h_0 = 1.0$, 0.9, 0.8, and 0.5 are presented in Figure 5. Case A is the one described above, but it has been included so that direct comparisons can be made with the other cases. When $H_0/h_0 < 0.5$, the response at this sinuosity is essentially that for a flat-bedded channel, which can be seen in Figure 10*b*; hence these results have not been included in the figure.

As the bed topography is damped, the region of crossing of the boundary shear stress maximum from near the inside to near the outside bank is shifted from the center of the bend to its downstream end. Moreover, the highest values of the bottom stress move inward in position from the upstream side to the top of the point bar. Also, the net outward velocity over the bar decreases to zero, permitting the helical flow to spread toward the inner bank. If the bed topography in a sediment-transporting stream were reduced in a similar manner, the changing pattern in boundary shear stress would cause rapid deposition at the downstream end of the point bar and rapid erosion at the downstream end of the pool, reinstating the characteristic topography. At first the new bar would be situated downstream of the radius-of-curvature minimum, but as the bar grew, convective acceleration would cause the zones of deposition and erosion to shift upstream until the top of the bar was at the radius-of-curvature minimum. At this location the outward flow (and sediment transport) over the top of the point bar would be reestablished, and the upstream drift of the deposition zone would be terminated. In contrast, if the bar were too large or too far upstream, the free-surface slope producing the outward flow component would be enhanced, and the upstream face of the bar would erode.

Although the pattern of bed topography has a substantial effect on the velocity field, it is the bottom roughness parameter that primarily controls the magnitude of the bottom stress and hence the sediment-transport rates. Outputs from calculations employing $\zeta_0 = 3.16 \times 10^{-4}$, 1.0×10^{-3}, and 3.16×10^{-3} are compared in Figure 6. These results clearly show that increasing ζ_0 substantially increases both the magnitude of the boundary shear stress and that of the downstream, but not the cross-stream, bottom stress component. This means that as ζ_0 increases, the deflection of flow from parallel to the stream centerline is somewhat decreased. Nevertheless, the primary effect of ζ_0 is as a control on the magnitude of $[(\tau_{zs})_\eta]_{av}/\rho U^2$. This occurs through α, which depends on F_1. Similarly, the magnitude of α depends on the distribution of turbulent mixing in the interior of the flow and hence on the nondimensional eddy coefficient ($\kappa = K/u_* h_0$) that is used.

Four possible choices for κ are shown in Figure 7. These are presented graphically along with the resulting velocity profiles for steady, horizontally uniform flow. In each case, as the maximum value of κ increases, so does the position of the maximum relative to the bottom, producing less shear in the resulting velocity profiles. Although the profile labeled B is the one most commonly used for channel flows, C provides somewhat greater coupling between layers, as might occur in a broad, shallow stream with numerous bed irregularities capable of producing boils and other large-scale mean-momentum-transferring motions. These are common features in many meandering streams, so most of the calculations presented in this paper have been based on $\kappa = k\zeta(1 - \zeta)^{1/2}$, as represented by C. The functional forms for A, B, and D, respectively, are $\kappa = k\zeta e^{-2\zeta}$, $\kappa = k\zeta(1 - \zeta)$, and $\kappa = k\zeta$. The limiting case of $k\zeta e^{-2\zeta}$ appears to give too much shear, whereas $\kappa = k\zeta$ seems to yield too little shear relative to that measured in meandering streams.

The various cases presented in Figure 8, labeled in correspondence with those of Figure 7, show that significant changes in flow pattern can arise owing to adjustments in the form of κ. This parameter affects the magnitude of the boundary shear stress relative to the ρU^2, with the largest stresses being given by $\kappa = k\zeta$, but more importantly it controls the intensity of the secondary circulation. Although the value of α depends on the functional form of κ, it is more sensitive to ζ_0 over the natural range of these two variables. In contrast, the amount and distribution of shear in the zero-order flow, and hence the degree of deflection of the near-surface and near-bottom velocities, are governed primarily by κ, as can be observed in Figure 8. With increased turbulent mixing the patterns of both the vector bottom stress and the surface velocity show a reduction in cross-stream relative to downstream in-

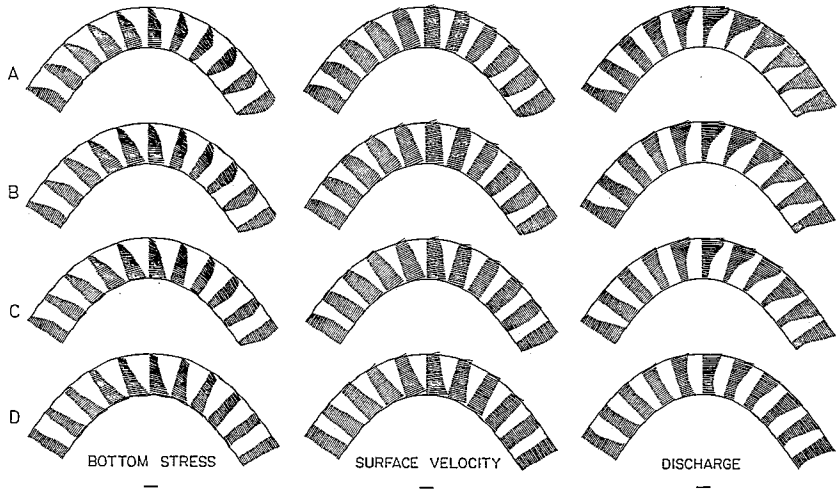

Fig. 5. Change in flow variables as the characteristic bed topography is decreased in magnitude. The values of H_0/h_0 are (*a*) 1.0, (*b*) 0.9, (*c*) 0.8, and (*d*) 0.5. Note the extreme sensitivity of the boundary shear stress distribution to bed topography, hence the inappropriateness of flat bed results to natural streams.

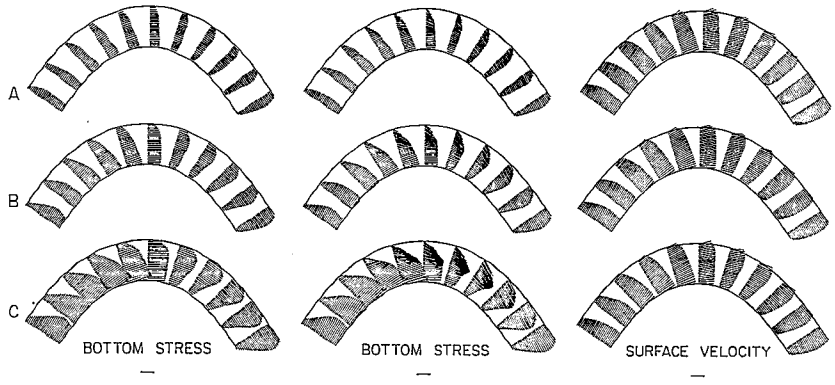

Fig. 6. Change in flow variables with z_0/h_0. The values of this parameter that were used are (*a*) 3.2×10^{-4}, (*b*) 1.0×10^{-3}, and (*c*) 3.2×10^{-3}. Note that the primary effect of increasing the nondimensional bottom roughness parameter is to decrease the magnitude of the response, the general flow patterns being relatively insensitive to such variations.

tensity, that is, they show a substantially decreased secondary circulation everywhere in the channel.

The effects of channel curvature on a flow with natural bed geometry are shown in Figure 9, while the effects on a flat-bedded flow are given in Figure 10. Comparison of these two figures makes clear the importance of bed topography at all sinuosities, especially in crossings, where a well-developed low-velocity region on the up-valley side of the stream is seen only in the former case. In addition, the outward bottom stress over the top of the point bar, although reduced for $\omega = 105°$, is entirely replaced by a strong inward component in all of the flat-bedded situations.

For the cases in Figure 9, the zone of high boundary shear stress crosses from near the inside bank to the outside of the stream in the neighborhood of the minimum radius of curvature. In contrast, for all of the flat-bedded cases this zone of high boundary shear stress remains near the inner bank until the downstream crossing. This fundamental difference between flows in channels with flat bottoms, or bottoms without downstream cross-sectional variation, and those in channels with natural topography, makes it very difficult to transfer the numerous results of flume experiments in the former types of systems to erodible-bed tidal channels and to rivers. *C. Yen* [1967] previously made this point after comparing the results of his laboratory investigation of flow through a bend of constant curvature with equilibrium bar-pool topography to results obtained by *B. Yen* [1965] in the same channel but with a flat bed. Unfortunately, our calculations show that the problem remains even at higher sinuosities.

SUMMARY AND CONCLUSIONS

The calculations presented in this paper demonstrate that accurate models of sediment-transporting flows in meandering streams must (1) either employ an appropriate curvilinear coordinate system or include convective accelerations associated with the curved stream path and (2) take account, in the lowest order, of convective accelerations induced by the large-scale bed topography characteristic of such systems. Using data from Hooke's fixed-bed run (in order to avoid complications associated with shallow flow over complex bed-form

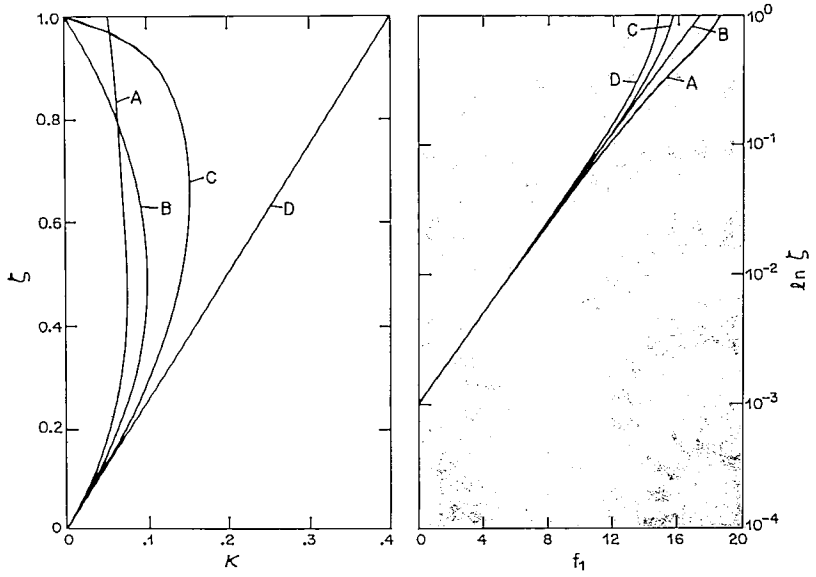

Fig. 7. Nondimensional eddy viscosity (κ) and corresponding nondimensional velocity (f_1) profiles. The former are plotted in a linear fashion, whereas the latter are drawn using semilogarithmic coordinates. The pertinent functions are (*a*) $\kappa = k\zeta e^{-2\zeta}/\mu$, (*b*) $\kappa = k\zeta(1-\zeta)$, (*c*) $\kappa = \kappa\zeta(1-\zeta)^{1/2}$, and (*d*) $\kappa = d\zeta$. Note that these are listed in the order of increasing elevation of the location of the maximum value, as well as in the order of increasing magnitude of the maximum value. Von Karman's constant is set at 0.40.

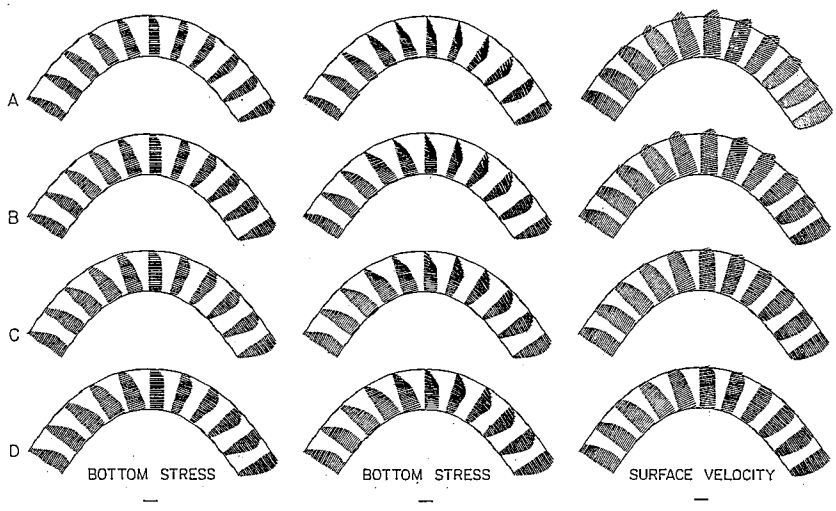

Fig. 8. Variation of flow properties with often-used functional forms for κ. These are labeled as in Figure 7; therefore, Figure 8*a* represents the case with the least turbulent mixing (least coupling between levels in the flow) and Figure 8*d* represents the case with the greatest. The main effects are an increased average boundary shear stress and a reduced secondary circulation with increased turbulent mixing.

fields), a model that includes these features has been shown to produce realistic fields of free-surface elevation and boundary shear stress. Our flow model then was used to show that bed topography plays a dominant role in typical channels with sine-generated-curve traces characterized by $\omega < 55°$ or so, but that channel curvature is of equal or greater importance when ω exceeds this value.

In addition, we have shown that specific flow characteristics can be related, at least qualitatively, to particular external parameters in channels with typical topographic features. For example, under these conditions the magnitude of the boundary shear stress, and hence of the sediment-transport rate, is determined primarily by the channel roughness, whereas the intensity of the secondary circulation is determined primarily by the vertical structure of the turbulent-mixing coefficient. Similarly, the importance of topographically induced convective accelerations depends on the height of the bar or depth of the pool relative to the mean depth, and the magnitude of flow enhancement on the inside of the bend depends on the degree of curvature. The effect of topographically induced convective accelerations is to cause the maximum boundary shear stress (hence sediment-transport rate) to cross from the inside to the outside of the bend in the region of minimum radius of curvature, whereas the effect of flow enhancement on the inside of the bend is to keep the maximum bottom-stress zone against the inside bank for a substantial distance beyond this point. Other things being equal, curvature is more important in a wide stream than in a narrow one, so the sediment-transport patterns can be expected to be fairly different in these two cases.

Externally induced variation in the complex interplay among important flow characteristics can substantially alter

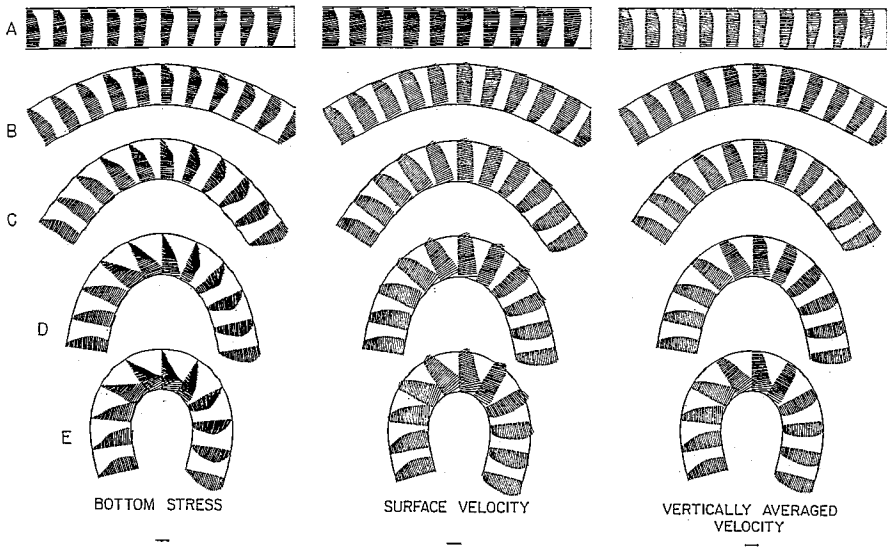

Fig. 9. Variation of flow properties with sinuosity in a channel with typical bed topography. The values of ω in this figure are (*a*) 0°, (*b*) 30°, (*c*) 55°, (*d*) 80°, and (*e*) 105°. Note that bed topography effects dominate over those due to channel curvature for $\omega < 30°$ or so, whereas the curvature becomes quite important for $\omega < 55°$.

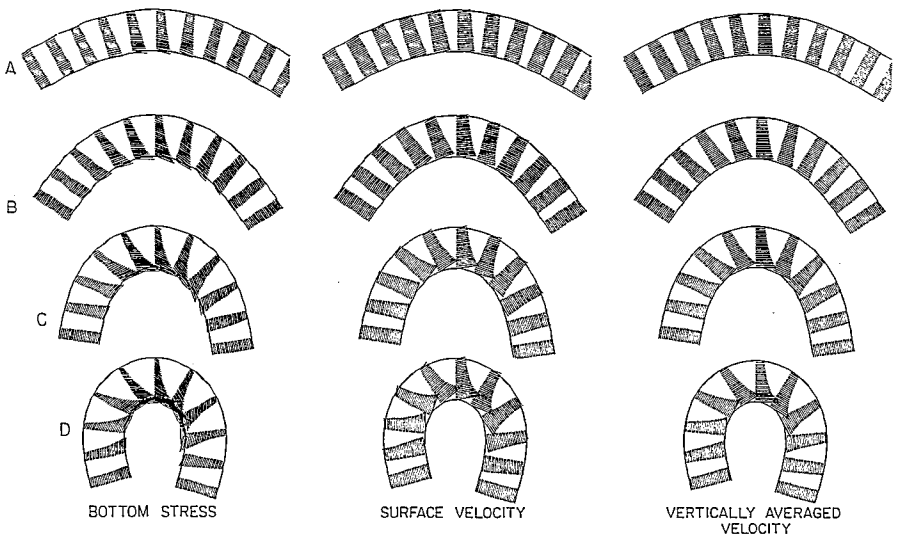

Fig. 10. Variation of flow properties with sinuosity in a flat bedded channel. The values of ω in this figure are (*a*) 30°, (*b*) 55°, (*c*) 80°, (*d*) and 105°. Flow in a straight channel with a flat bed has only vertical structure, so this case has not been included. Comparison with the previous figure permits a qualitative evaluation of the effects of channel topography versus those of channel curvature at high sinuosity.

patterns of boundary shear stress in natural sediment-transporting systems; hence they can change the erosion-deposition patterns and result in adjustments toward new equilibrium states. In order to examine the path that these adjustments take or even to investigate the nature and stability of the ultimate balance that is achieved among the relevant geometric and flow variables, a reasonably accurate flow model is essential.

APPENDIX: DERIVATION OF HORIZONTAL EQUATIONS OF MOTION

If the centerline of the channel is defined in Cartesian coordinates by $(x, y) = (x_0(s), y_0(s))$, the radius of curvature of the channel centerline at any point is given by

$$R = R(s) = \left(\frac{dx_0}{ds}\frac{d^2y_0}{ds} - \frac{d^2x_0}{ds}\frac{dy_0}{ds}\right)^{-1} \tag{A1}$$

Using the definition sketch in Figure 1, for which R begins positive and then becomes negative, the curvilinear coordinate system can be related to the Cartesian one by

$$x = x_0 - \Delta x = x_0 - n\cos\beta = x_0 - n\frac{dy_0}{ds} \tag{A2a}$$

$$y = y_0 + \Delta y = y_0 + n\sin\beta = y_0 + n\frac{dx_0}{ds} \tag{A2b}$$

In these curvilinear coordinates the scale factors associated with the cross-stream and vertical directions are unity, but the one associated with the downstream direction is

$$h_s = \left[\left(\frac{\partial x}{\partial s}\right)^2 + \left(\frac{\partial y}{\partial s}\right)^2 + \left(\frac{\partial z}{\partial s}\right)^2\right]^{1/2}$$

$$= 1 - \frac{n}{R} = 1 - N \tag{A3}$$

Employing all three scale factors and writing the relevant unit vectors as $\mathbf{e}_s$, $\mathbf{e}_n$, and $\mathbf{e}_z$ permits the inertial term of the equation of motion to be written

$$\rho u\cdot\nabla u = \rho\left[\frac{u_s}{1-N}\frac{\partial u_s}{\partial s} + u_n\frac{\partial u_s}{\partial n} + u_z\frac{\partial u_s}{\partial z} - \frac{u_s u_n}{(1-N)R}\right]\mathbf{e}_s$$
$$+ \rho\left[\frac{u_s}{1-N}\frac{\partial u_n}{\partial s} + u_n\frac{\partial u_n}{\partial n} + u_z\frac{\partial u_n}{\partial z} + \frac{u_s^2}{(1-N)R}\right]\mathbf{e}_n$$
$$+ \rho\left[\frac{u_s}{1-N}\frac{\partial u_z}{\partial s} + u_n\frac{\partial u_z}{\partial n} + u_z\frac{\partial u_z}{\partial z}\right]\mathbf{e}_z \tag{A4}$$

and the divergence of the deviatoric stress to be expressed as

$$\nabla\cdot\tilde{\tau} = \left[\frac{1}{1-N}\frac{\partial}{\partial s}\tau_{ss} + \frac{\partial}{\partial n}\tau_{ns} + \frac{\partial}{\partial z}\tau_{zs} - \frac{2\tau_{ns}}{(1-N)R}\right]\mathbf{e}_s$$
$$+ \left[\frac{1}{1-N}\frac{\partial}{\partial s}\tau_{ns} + \frac{\partial}{\partial n}\tau_{nn} + \frac{\partial}{\partial z}\tau_{zn} + \frac{\tau_{ss}-\tau_{nn}}{(1-N)R}\right]\mathbf{e}_n$$
$$+ \left[\frac{1}{1-N}\frac{\partial}{\partial s}\tau_{zs} + \frac{\partial}{\partial n}\tau_{zn} + \frac{\partial}{\partial z}\tau_{zz} - \frac{\tau_{zn}}{(1-N)R}\right]\mathbf{e}_z \tag{A5}$$

Here u_s, u_n, and u_z are the velocity components in the three curvilinear coordinate directions and τ_{ss}, τ_{ns}, τ_{zs}, τ_{nn}, τ_{zn}, τ_{zz} are the six unique components of the deviatoric stress τ, written in this frame of reference, and ρ is the density of the fluid. The gradient of the pressure field is given by

$$\nabla p = \frac{1}{1-N}\frac{\partial p}{\partial s}\mathbf{e}_s + \frac{\partial p}{\partial n}\mathbf{e}_n + \frac{\partial p}{\partial z}\mathbf{e}_z \tag{A6}$$

The deviatoric stress can be expressed in terms of the strain rate tensor $\tilde{S}$ and a scalar, kinematic eddy viscosity K in systems for which the diffusion of momentum is primarily in the vertical direction and for which the horizontal transfer of momentum is of little importance in the overall force balance or for which it is fully characterized by the theory. In the case at hand these criteria are satisfied, so we can write $\tilde{\tau} = 2\rho K\tilde{S}$, where ρ is the fluid density. This yields

$$\tau_{ss} = 2\rho K\left(\frac{1}{1-N}\frac{\partial u_s}{\partial s} - \frac{u_n}{(1-N)R}\right)$$

$$\tau_{nn} = 2\rho K\left(\frac{\partial u_n}{\partial n}\right)$$

$$\tau_{zz} = 2\rho K\left(\frac{\partial u_z}{\partial z}\right)$$

$$\tau_{ss} = \rho K\left(\frac{1}{1-N}\frac{\partial u_z}{\partial s} + \frac{\partial u_s}{\partial z}\right) \tag{A7}$$

$$\tau_{zn} = \rho K\left(\frac{\partial u_z}{\partial n} + \frac{\partial u_n}{\partial z}\right)$$

$$\tau_{ns} = \rho K\left(\frac{1}{1-N}\frac{\partial u_n}{\partial s} + \frac{u_s}{(1-N)R} + \frac{\partial u_s}{\partial n}\right)$$

Substituting these expressions for the components of $\tilde{\tau}$ into (A5) and equating the result to (A4) plus (A6) gives an appropriate equation of motion. Separating this into component equations, assuming steady flow, and taking ρ to be constant yield the following expression for the downstream components of force per unit mass:

$$\frac{u_s}{(1-N)}\frac{\partial u_s}{\partial s} + u_n\frac{\partial u_s}{\partial n} + u_z\frac{\partial u_s}{\partial z} - \frac{u_s u_n}{(1-N)R}$$

$$= -\frac{1}{\rho(1-N)}\frac{\partial p}{\partial s}$$

$$+\frac{2}{(1-N)}\frac{\partial}{\partial s}\left[K\left(\frac{1}{(1-N)}\frac{\partial u_s}{\partial s} - \frac{u_n}{(1-N)R}\right)\right]$$

$$-\frac{2K}{(1-N)R}\left(\frac{1}{(1-N)}\frac{\partial u_n}{\partial s} + \frac{\partial u_s}{\partial n} + \frac{u_s}{(1-N)R}\right)$$

$$+\frac{\partial}{\partial n}\left[K\left(\frac{1}{(1-N)}\frac{\partial u_n}{\partial s} + \frac{\partial u_s}{\partial n} + \frac{u_s}{(1-N)R}\right)\right]$$

$$+\frac{\partial}{\partial z}\left[K\left(\frac{1}{(1-N)}\frac{\partial u_z}{\partial s} + \frac{\partial u_s}{\partial z}\right)\right] \tag{A8a}$$

For the cross-stream components we get

$$\frac{u_s}{(1-N)}\frac{\partial u_n}{\partial s} + u_n\frac{\partial u_n}{\partial n} + u_z\frac{\partial u_n}{\partial z} + \frac{u_s^2}{(1-N)R}$$

$$= \frac{-1}{\rho}\frac{\partial p}{\partial n} + \frac{1}{(1-N)}\frac{\partial}{\partial s}\left[K\left(\frac{1}{(1-N)}\frac{\partial u_n}{\partial s} + \frac{\partial u_s}{\partial n} + \frac{u_s}{(1-N)R}\right)\right]$$

$$-\frac{2K}{(1-N)R}\frac{\partial u_n}{\partial n} + \frac{2K}{(1-N)R}\left[\frac{1}{(1-N)}\frac{\partial u_s}{\partial s} - \frac{u_n}{(1-N)R}\right]$$

$$+2\frac{\partial}{\partial n}\left(K\frac{\partial u_n}{\partial n}\right) + \frac{\partial}{\partial z}\left[K\left(\frac{\partial u_z}{\partial n} + \frac{\partial u_n}{\partial z}\right)\right] \tag{A8b}$$

NOTATION

F_m channel Froude number times $(m_0/l_0)^{1/2}$.
F_r channel Froude number $U/(gh_0)^{1/2}$.
F_1 average of the velocity profile function f_1 over the flow depth.
F_2 average of the profile function f_2 over the flow depth.
H_0 elevation difference between base of pool and top of point bar.
K kinematic eddy viscosity.
K_0 zero-order kinematic eddy viscosity.
K_1 first-order kinematic eddy viscosity.
K_2 second-order kinematic eddy viscosity.
N cross-stream coordinate divided by radius of curvature (n/R).
N_0 value of N at the upstream crossing.
Q_n component of discharge, per unit width in the cross-stream direction.
Q_s component of discharge per unit width in the downstream direction.
R radius of curvature of the centerline of the stream.
R_0 minimum radius of curvature of the centerline of the stream.
$\tilde{S}$ strain rate tensor.
U cross sectionally averaged velocity $(\mathcal{Q}/h_0w_0)$.
b_1 magnitude of the n coordinate at the inner bank.
b_2 magnitude of the n coordinate at the outer bank.
$\mathbf{e}_n$ unit vector in the cross-stream direction.
$\mathbf{e}_s$ unit vector in the downstream direction.
$\mathbf{e}_z$ unit vector in the near-vertical direction (perpendicular to the s, n plane).
f_1 zero-order velocity profile with distance from the bed.
f_2 profile function defined by (43).
g acceleration due to gravity.
h local depth of flow.
h_0 mean depth of flow.
h_s scale factor associated with the downstream coordinate direction.
k von Karman's constant.
m_0 half wavelength measured along the channel centerline.
n cross-stream coordinate.
p pressure.
p_a atmospheric pressure.
r radial coordinate.
s downstream coordinate.
u_n velocity component in the cross-stream direction.
u_s velocity component in the downstream direction.
u_z velocity component in the near-vertical direction.
u_* shear velocity.
$(u_*)_n$ shear velocity component in the cross-stream direction.
$(u_*)_s$ shear velocity component in the downstream direction.
w_0 mean width.
x down-valley coordinate.
x_0 down-valley coordinate of the channel centerline.
y cross-valley coordinate.
y_0 cross-valley coordinate of the channel centerline.
z near-vertical coordinate (perpendicular to the s, n plane).
z_0 bottom roughness parameter.
l_0 centerline surface elevation change between adjacent crossings.
σ value of z at the free surface of the stream.
σ_* value of s defined by (37).
σ_c value of s at the channel centerline.
$\mathcal{Q}$ magnitude of the discharge.
$\langle\ \rangle$ average of a variable over the flow depth.
$\hat{\ }$ variable nondimensionalized as indicated in (26).
$(\ )_\eta$ variable evaluated at the stream bed.
α ratio of $(\tau_{zs})_\eta{}^0$ to $\rho\langle u_s\rangle^2$.
β angle relating ds to dx_0 and dy_0 (see Figure 1).
γ_1 parameter defined by (16a).
γ_2 parameter defined by (16b).
ζ distance above the stream bed nondimensionalized by the local depth.
ζ_0 roughness parameter nondimensionalized by the local depth.
η value of the z coordinate at the bed.

θ circumferal coordinate.
κ nondimensional zero-order eddy viscosity profile.
ρ density of the fluid.
σ parameter with value of $+1$ when τ_{zs} is positive and $-$ when τ_{zs} is negative.
$\tilde{\tau}$ deviatoric stress tensor.
τ_{ij} components of the deviatoric stress tensor.
τ_{nn} normal stress in the cross-stream direction.
τ_{ns} shear stress in the downstream direction on a cross-stream plane.
τ_{ss} normal stress in the downstream direction.
τ_{zz} normal stress in the near-vertical direction.
τ_{zn} shear stress on the z plane in the cross-stream direction.
τ_{zs} shear stress on the z plane in the downstream direction.
$(\tau_{zs})_0$ boundary shear stress at $s = 0$.
ϕ angle of local stream centerline with respect to down-valley direction.
ω value of ϕ where the down-valley axis is crossed.

Acknowledgments. This research was supported by National Science Foundation grant ENG 7816977. We wish to thank Bill Dietrich for numerous lengthy discussions concerning the processes that this paper attempts to model and Pat Wiberg for checking the equations.

REFERENCES

DeVriend, H. J., and H. J. Geldof, Main flow velocity in short river bends, *J. Hydraul. Div. Am. Soc. Civ. Eng.*, *109*(7), 991–1011, 1983.
Dietrich, W. E., Flow, boundary shear stress, and sediment transport in a river meander, Ph.D. dissertation, 261 pp., Dep. of Geol. Sci., Univ. of Wash., Seattle, 1982.
Dietrich, W. E., and J. D. Smith, Influence of the point bar on flow through curved channels, *Water Resour. Res.*, *19*, 1173–1192, 1983.
Engelund, F., Flow and bed topography in channel bends, *J. Hydraul. Div. Am. Soc. Civ. Eng.*, *HY11*, 1631–1648, 1974.
Hooke, R. LeB., Distribution of sediment transport and shear stress in a meander bend, *J. Geol.*, *83*, 543–565, 1975.
Kalkwijk, J. P. Th., and H. J. DeVriend, Computation of the flow in shallow river bends, *J. Hydraul. Res.*, *18*(4), 327–342, 1980.
Langbein, W. B., and L. B. Leopold, River meanders—Theory of minimum variance, *U.S. Geol. Surv. Prof. Pap.*, *422-H*, H1–H15, 1966.
Rozovskii, I. L., *Flow of Water in Bends of Open Channels* (in Russian), Academy of Sciences of the Ukranian SSR, Kiev, 1957. (English translation by Y. Prushansky, 233 pp., Israel Program for Scientific Translation, Jerusalem, 1961).
Yen, B., Characteristics of subcritical flow in a meandering channel, Ph.D. dissertation, 149 pp., Univ. of Iowa, Iowa City, 1965.
Yen, B. C., Spiral motion of developed flow in wide curved open channels, in *Sedimentation* (Einstein Volume), edited by H. W. Shen, chap. 22, Water Resources Publications, Fort Collins, Colo., 1972.
Yen, C., Bed configuration and characteristics of subcritical flow in a meandering channel, Ph.D. dissertation, 123 pp., Univ. of Iowa, Iowa City, 1967.
Yen, C., and B. Yen, Water surface configuration in channel bends, *J. Hydraul. Div. Am. Soc. Civ. Eng.*, *97*(HY2), 303–321, 1971.

S. R. McLean, Department of Mechanical and Environmental Engineering, University of California, Santa Barbara, CA 93106.
J. D. Smith, Geophysics Program AK-50, University of Washington, Seattle, WA 98195.

(Received November 1, 1982;
revised March 1, 1984;
accepted March 16, 1984.)